Automatic Separation of Basal Cell Carcinoma from Benign Lesions in Dermoscopy Images with Border Thresholding Techniques

Nabin K. Mishra[1], Ravneet Kaur[2], Reda Kasmi[3], Serkan Kefel[2], Pelin Guvenc[2], Justin G. Cole[1], Jason R. Hagerty[1,4], Hemanth Y. Aradhyula[4], Robert LeAnder[2], R. Joe Stanley[4], Randy H. Moss[4] and William V. Stoecker[1]

[1]*Stoecker and Associates, Rolla, MO, U.S.A.*

[2]*Southern Illinois University Edwardsville, Department of Electrical and Computer Engineering, Edwardsville, IL, U.S.A.*

[3]*University of Begaia, Department of Electrical Engineering, Bejaia, Algeria*

[4]*Missouri University of Science and Technology, Department of Electrical and Computer Engineering, Rolla, MO, U.S.A.*

{nkmhd3, stanleyj, hamcb, rhm, wvs, jrh55c}@mst.edu, {reet4ever, rdkasmi, serkankefel, bobleande1}@gmail.com, pelin.kefel@bioxconsulting.com, jgcole@iu.edu

Keywords: Basal Cell Carcinoma (BCC), Image Processing.

Abstract: Basal cell carcinoma (BCC), with an incidence in the US exceeding 2.7 million cases/year, exacts a significant toll in morbidity and financial costs. Earlier BCC detection via automatic analysis of dermoscopy images could reduce the need for advanced surgery. In this paper, automatic diagnostic algorithms are applied to images segmented by five thresholding segmentation routines. Experimental results for five new thresholding routines are compared to expert-determined borders. Logistic regression analysis shows that thresholding segmentation techniques yield diagnostic accuracy that is comparable to that obtained with manual borders. The experimental results obtained with algorithms applied to automatically segmented lesions demonstrate significant potential for the new machine vision techniques.

1 INTRODUCTION

The incidence of basal cell carcinoma (BCC) continues to rise worldwide, with incidence in the USA of all non-melanoma skin cancer exceeding 3 million cases, per year (Rogers et al., 2010). Morbidity and costs to society associated with advanced cases of BCC are significant. Costs of treatment for skin cancer more than doubled from 1998 to 2006 (Rogers and Coldiron, 2013). Newer nonsurgical treatment techniques (Zeichner et al., 2011) applicable to earlier-appearing lesions, could be combined with automated diagnostic methods to diagnose small lesions and treat them earlier. Therefore, automatic diagnosis of early lesions could provide significant societal benefits.

Automated pre-biopsy diagnosis of BCC was first attempted in the 1980s, using clinical images (Moss et al., 1989). The advent of dermoscopy, provided superior images containing far more detail and created a proliferation of the signs that identify melanoma and non-melanoma skin cancer (Argenziano et al., 2003; Stolz et al., 2002; Soyer et al., 2007, Marghoob et al., 2012). A number of studies appeared using image analytic techniques to detect melanoma in dermoscopy images. Relatively few studies used image analytic techniques to identify structures in BCC, including ulcers, semitranslucency, telangiectasia, and pigmented structures (Kefel et al., 2012; Guvenc et al., 2013; Cheng et al., 2011; Cheng et al., 2012; Cheng et al., 2013).

Pre-biopsy diagnosis of BCC has also been attempted using multiple alternative approaches, that incorporate various novel technologies for acquiring images, including confocal microscopy (Castro et al., 2015; Ahlgrimm-Siess et al., 2009; Eberhardt et al., 2004), optical coherence tomography (OCT) (Duan et al., 2014; Avanaki et al., 2013; Castro et al., 2015), multispectral imaging (Zhang et al., 2000; Tehrani et al., 2007; Ly et al., 2009), chemical application and photodynamic methods (Won et al., 2007; Kopriva et al., 2007; Gambichler et al., 2008). Studies applying non-imaging techniques have utilized impedance (Beetner et al., 2003; Dua et al., 2004; Aberg et al., 2004) and Raman spectroscopy (Larraona-Puy et al., 2009; Nijssen et al., 2002).

K. Mishra N., Kaur R., Kasmi R., Kefel S., Guvenc P., G. Cole J., R. Hagerty J., Y. Aradhyula H., LeAnder R., Joe Stanley R., H. Moss R. and V. Stoecker W.
Automatic Separation of Basal Cell Carcinoma from Benign Lesions in Dermoscopy Images with Border Thresholding Techniques.
DOI: 10.5220/0006173601150123
In *Proceedings of the 12th International Joint Conference on Computer Vision, Imaging and Computer Graphics Theory and Applications (VISIGRAPP 2017)*, pages 115-123
ISBN: 978-989-758-225-7

However, all of these alternative approaches have disadvantages, including more expensive equipment, slower acquisition time, and in some cases, a steep learning curve before properly operating the equipment and interpreting results. Dermoscopy images are acquired quickly. Some approaches require a probe that cannot be used on the earliest-appearing BCCs which are as small as 1mm in diameter. Many clinics already have the apparatus needed for dermoscopy. So, digital dermoscopy analysis performed on common, conventional, gel-contact, non-polarized images have advantages over alternate methods in diagnosing BCC. The purpose of this study was to determine the feasibility of automatic differentiating BCC from benign lesions by combining image analytic techniques applied to dermoscopy images with patient information and general image information.

2 METHODS

2.1 Experimental Data Sets

This study analyzed 1023 digital, 1024x768-pixel, gel-contact, non-polarized, dermoscopy images of lesions acquired during the National Institutes of Health-funded study SBIR R44 CA-101639-02A2 2007-2009. This set of images included 305 BCC lesions of which 26 (8.5%) were infiltrative, 28 (9.2%) were superficial, and 1 (0.33%) was metatypical, or baso-squamous. BCC size, measured at the greatest diameter, ranged 1-45mm, with median size = 6mm. Of these lesions, 47/305 (15.4%) were ≤ 3mm. There were 176 (57.7%) on heads and necks, 43 (14.1%) on upper limbs, 24 (7.9%) on lower limbs, and 62 (20.3%) on patients' trunks. Only 88 (28.9%) of patients had concern about the lesions; and 111 (36.4%) of patients noted a change in their lesion. Also, included in this set were 718 benign images of which 290 (40.4%) were nevi, 89 (12.4%) were dysplastic nevi, 5 (0.7%) were sebaceous hyperplasia, and 124 (17.3%) were seborrheic keratoses, with the remainder having various benign diagnoses.

Lesion images were acquired at four clinics in Plantation FL, Rolla MO, Columbia MO and Stamford CT. The Phelps County Regional Medical Center Institutional Review Board (Rolla, Missouri) approved this research. Only two of the BCCs were not biopsied and examined by a dermatopathologist; these were diagnosed using confocal microscopy. All benign lesions were either biopsied, or serially-examined and determined to have no change.

2.2 Overall Approach

Our general approach was to apply digital image analysis techniques previously used in melanoma detection (Jella, 2004; Mishra, 2014; Mishra et al., 2016; Gutman et al., 2016; Codella et al., 2016; Kaushik et al., 2013; Stoecker et al., 2013; Stoecker et. al., 2015) to find dermoscopy features in images of BCC. To these features, two features specific to BCC were added: vascular blush / semitranslucency (Kefel et al., 2016) and vessels / telangiectasia (Cheng et al., 2011). The overall approach is shown in Figure 1.

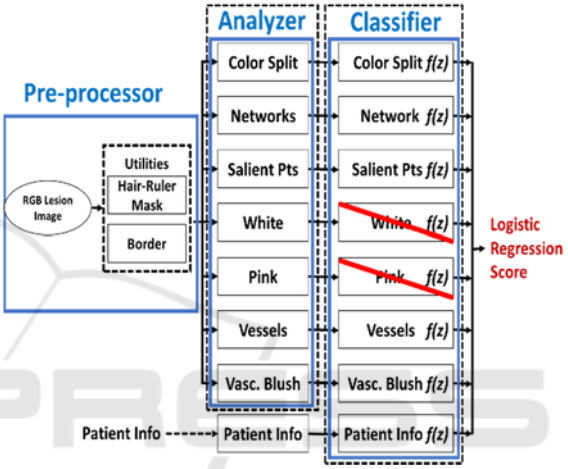

Figure 1: Overall system for BCC classifier. The seven image analyser modules are reduced to five modules at the classifier stage by logistic regression. The patient information module provides a sixth final module.

The final result is acquired with logistic regression using a leave-one-out cross validation technique.

The logistic regression function is defined by equation 1.

$$\varphi(z)=\frac{1}{1+e^{-z}} \quad \text{where} \quad z=\mathbf{W}^{T}\mathbf{X} \tag{1}$$

where X is a matrix with dimension d and W contains the weights for X. The desired hypothesis can be achieved by minimizing the equation 2 using iterative gradient approach (Abu-Mostafa et al., 2012).

$$E_{in}=\frac{1}{N}\sum_{n=1}^{N}\log(1+e^{-y_n\mathbf{W}^{T}\mathbf{X}_n}) \tag{2}$$

where N is the No. of samples, y_i will be either one or zero for positive and negative set respectively.

2.3 Border Generating Methods

This research applied six different lesion border segmentation algorithms based on five different thresholding algorithms (Kaur et al., 2016). The pre- and post-processing for these algorithms is shown in Figure 2. The first thresholding method, based on work by Huang and Huang, minimizes the fuzziness measure of a dermoscopy skin lesion image (Landini, 2013; Huang and Huang, 1995) (Huang, Figure 2).

The next skin lesion segmentation algorithm based on work by Li and Tam, was based on minimum, cross-entropy thresholding, where threshold selection was done by minimizing the cross entropy between the dermoscopy image and its segmented version (Landini, 2013; Li and Tam, 1998) (Li, Figure 2).

Finally, an effective image information measure was obtained by modifying an image entropy-measure-based thresholding method; this helped obtain two more lesion borders using the assistance of different pre-processing and post-processing methods (Landini, 2013; Shanbhag, 1994) (Shanbhag-1 and -2, Figure 2).

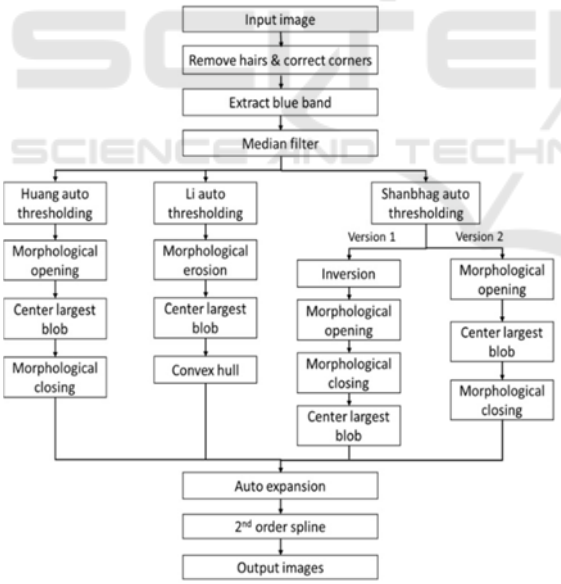

Figure 2: Flowchart for Huang, Li and Shanbhag algorithms. Isodata and Otsu methods follow Shanbhag-2.

Kaur et al. also discussed that Otsu (Otsu, 1979) and Isodata (Riddler and Calvard, 1978) methods produced borders similar to Huang, Li and Shanbhag borders. From the four algorithms in Figure 2, Shanbhag-2 pre- and post-processing provided the best results for Otsu and Isodata thresholding methods.

Hair removal is a crucial pre-processing step used in all the algorithms. The hair removal technique (Kasmi, 2016) was developed by converting an image to grayscale and then scanned by a horizontal array of 1x7 pixels; if the difference between the smallest and the largest pixel values was more than 15, then the smallest pixel indicated the presence of hair. On the identified hair segment, three horizontally-oriented parallel masks were centered and replaced by the average of the two adjacent masks. This process is followed by the same procedure using a vertical array. The final mask is subtracted from the grayscale image following a binary thresholding to produce the hair mask. This mask undergoes multiple morphological operations and the linear interpolation inpainted technique is applied to remove the unwanted hairs (Kasmi, 2016). An example of hair removal can be seen in Figure 3.

Figure 3: Example for hair removal. (a) Image with hairs, (b) Image after hair removal.

The two utilities above, hair removal and image segmentation to determine the border, were applied to each image prior to processing for the following lesion structures.

2.4 General Lesion Network Structure

2.4.1 Atypical Pigment Network Detection

Benign melanocytic nevi usually contain a visible pigment network that is either fairly symmetric and regular, or atypical. A pigment network whose network structure varies in size and shape is called an “irregular” or “atypical pigment network” (APN). Different varieties of irregular wide/or dark APN aberrations may be appear as brown, black, gray meshes or thick lines in dermoscopy images (Argenziano et al., 1998). The variance detection method for APN summarized here is described in Mishra, 2014). Nearly all APN areas have relatively high variance in the relative-red plane, obtained by subtracting the average red value of surrounding skin from the red values in the RGB image. The relative-red plane is divided into 16x16 blocks.

Blocks where variance falls above an adaptive threshold calculated using the mean and standard deviation of variance among all the 16x16 blocks of the lesion, are candidates for APN. Because granularity (Braun et al., 2007) can mimic APN, a green-to-blue ratio threshold was used to remove the false positive granular structures that were detected as APN. Figure 4 shows (a) an image of a benign lesion having an APN and (b) the lesion's APN enhanced with an overlay. Features such as atypical area size and asymmetry are used to measure APN. The pigment network of the benign melanocytic nevus in Figure 4, is reasonably symmetrical and was correctly identified as benign.

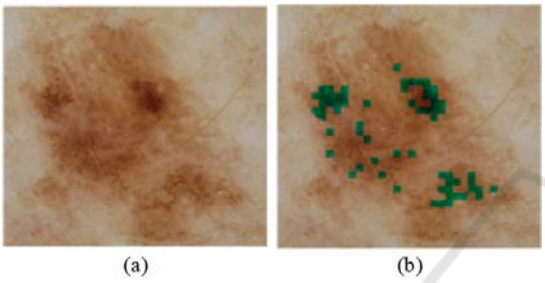

Figure 4: Benign lesion with APN overly. (a) Original image, (b) APN overlay.

2.4.2 Salient Point Detection

"Salient points" are those points which are detected using Steger's method of line detection (Steger, 1996). Dark lines in an image have a low first order derivative in the direction of the line, and a high second derivative in the orthogonal direction. The best results of trials performed in discriminating melanoma were obtained by using the intensity plane ((R+G+B)/3) to detect salient points (Jella, 2004). The method is best implemented by first smoothing, or blurring the intensity image with a Gaussian filter, as a pre-processing step. The choice of the filter sigma can significantly affect the outcome. 1.02 was experimentally found to be sigma's optimal value (Jella, 2004). After finding the salient points, they were used to calculate various texture and color features that would help detect melanoma. Salient points used that way tend to favor sharp edges of dark structures.

2.5 General Lesion Structure 3: Color Segmentation by Median Split Technique

"Median split" is a pixel-clustering method that is based on the characteristics of an image's histogram (Heckbert, 1982; Umbaugh et al., 1989; Umbaugh, 2010; Kaushik et al., 2013). The method was originally used in the development of an image compression technique (Heckbert, 1982). In this present application, after the lesion border was used to segment the lesion from the rest of the dermoscopy image, the median split algorithm was applied to pixels in the area of the lesion. To apply the technique, first, all lesion-area pixels are considered to be in a single color bin that has R, G and B dimensions. The dimension having the largest range is then split at the median color, such that the two resulting bins have equal numbers of pixels. Each iteration first considers the ranges of the colors in each bin, and then splits the bin having the largest range into two bins having equal pixel populations. The bin with the highest range on any color axis is chosen for the subsequent split. Within the chosen bin, the split is performed along the color axis having the highest range. In this study, three iterations were performed, resulting in a lesion's segmentation into four color regions. Each region was then represented by its average color. Figure 5 illustrates the results of a median split obtained from the original RGB image of a benign nevus. Note that the lesion mask was applied to the RGB image, before applying the median split algorithm, so that only the lesion colors were split. Note also, that the symmetry and radial gradient of the colors were captured using the median split algorithm.

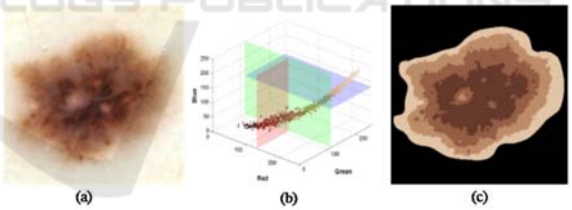

Figure 5: Median split segmentation performed by subsequent splitting of the plane with highest range. (a) Original dermoscopy image, (b) Histogram, (c) Median split image.

2.6 BCC Structure

2.6.1 Telangiectasia Detection

The small blood vessels seen in basal cell carcinomas are called telangiectasia (Argenziano et al., 2003). An algorithm for telangiectasia detection was implemented in (Cheng et al., 2011). In the most advanced case, telangiectasia takes the form of wider vessels branching into smaller vessels like a tree does; consequently, that process is called "arborizing" telangiectasia. Non-arborizing

telangiectasia are more common and seen in the earlier development of BCC. The presence of vessels alone is not significant, because wide telangiectasia may be seen in any sun-damaged skin (Figure 6a, on the upper right). The detection technique uses drops at 45-degree directions from a pixel. If drop thresholds for a given pixel distance are met, then a candidate telangiectasia pixel is present (Figure 6b). Because bubble and hair noise can interfere with telangiectasia detection, a separate hair mask was applied, first. This telangiectasia detection method was used to remove the bubble noise (Figure 6c) and consequently find the telangiectasia in Figure 6d.

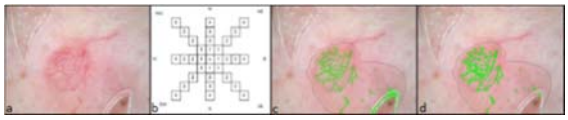

Figure 6: (a) Telangiectasia, (b) Cheng drop algorithm, (c) Bubble noise (d) Bubble noise removed.

2.6.2 Semitranslucency Detection

Smooth areas known as semitranslucencies are useful in detecting BCC (Stoecker et al., 2009). Distinguishing these areas from other areas depends critically on features of color and smoothness (Cheng et al., 2011; Cheng et al., 2012). To implement automatic detection, smoothness- and color-based filtering was employed with the use of control limits by (Kefel et al., 2016). Example images showing semitranslucency detection in BCC are shown in Figure 7.

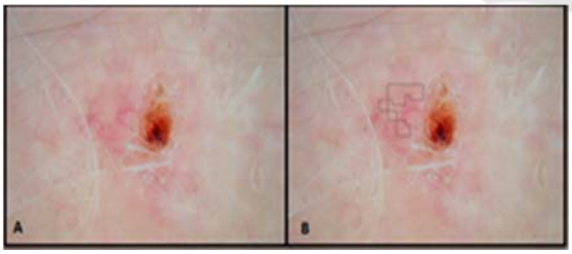

Figure 7: BCC with detected smooth semitranslucent areas found automatically.

2.7 Final Stage: Demographic-feature Data Incorporation

Data recorded for each patient included age in years, gender, lesion size, lesion location (head/neck, abdomen, chest, back, upper extremities, lower extremities), changes noted in the lesion (yes/no), concern about the lesion (yes/no), and patient location (2 values, residing within 30 degrees of the equator or not).

3 RESULTS

3.1 Performance of BCC Diagnostic Model with Different Borders

The logistic regression models for each of the six modular components in the final decision model were constructed using a leave-one-out cross validation technique via the Logit procedure, in the SAS software environment (SAS Institute Inc. Cary, NC). These models were then combined into a single logistic regression model that would separate 305 BCC from 718 competing, benign lesions. SAS's Logistic regression model applies the leave-one-out technique to separate the training set from the test set one-by-one, to effect model construction. The decision accuracy for the model is the maximum obtained over the possible logistic probabilities, which range 0-1. Results of the mean decision accuracy are shown for the six automatic border techniques and manual borders, Figure 8.

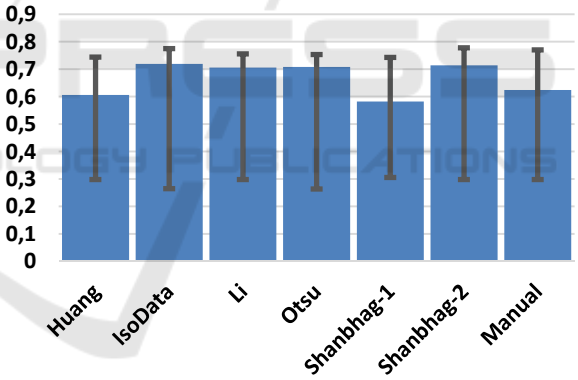

Figure 8: Mean diagnostic accuracy vs. border method, with errors bars shown.

The average diagnostic performance obtained using the dermatologist expert-determined border is slightly exceeded by the diagnostic performance using two of the automatic borders methods: Isodata and Shanbhag-2.

3.2 XOR Error for Automatic Borders

There are significant differences between the automatic borders and the manual dermatologist borders. The XOR border difference, which counts the total pixel error and divides by the total manual (dermatologist) border is defined in Equation 3

(Celebi et al., 2009; Celebi et al., 2015; Hance et al., 1996).

$$\text{XOR Error} = \frac{\text{Area}(AM \oplus MM)}{\text{Area}(MM)} = \frac{FP+FN}{TP+FN} \quad (3)$$

where AM = Automatic border mask, MM = Manual border mask, and $\oplus$ symbolizes the logical XOR between the two masks. Respectively, FN and FP are the lesion and non-lesion pixels falsely detected; TP and TN are the lesion and non-lesion pixels correctly detected, where "lesion", indicates the manual border (Kaur et al., 2016). The average difference between the automatic borders measured by XOR error is shown in Figure 9.

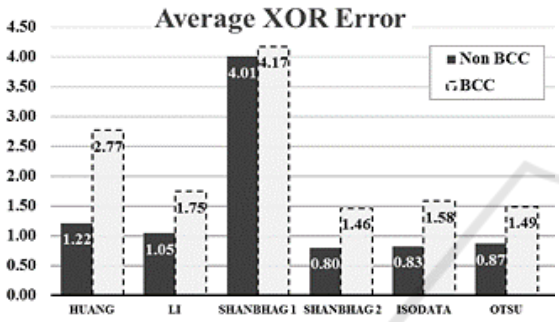

Figure 9: Average XOR error for 6 methods.

This XOR error exceeds four, i.e. quadruple the lesion area, in the case of Shanbhag-1 borders. Overall all XOR errors for BCC segmentation exceed 1.46 for BCCs. This implies that the segmentations are quite different. The average XOR difference between automatic and manual borders is greater than the lesion area. Examples of automatic borders are given, Figure 10.

XOR error under-represents the FN errors and over-represents the FP errors, Sforza et al. developed the relative XOR error for border inaccuracy measure using equation 4. (Sforza et al., 2012, Kaur et al., 2016)

$$\text{Relative XOR Error} = \frac{FN}{TP+FN} + \frac{FP}{FP+TN} = \left(1 - \frac{TP}{TP+FN}\right) + \left(1 - \frac{TN}{TN+FP}\right) \quad (4)$$

where *FN/(TP+FN)* and *FP/(FP+TN)* are the *FN* and *FP* ratios, respectively. *FN* and *FP* ratio can also be represented as sensitivity and specificity respectively by the two fraction terms in the right in equation 4. Using the relative XOR error, Kaur et al. developed lesion capture ratio using the weights ω from the manual grading shown in equation 5. (Kaur et al., 2016)

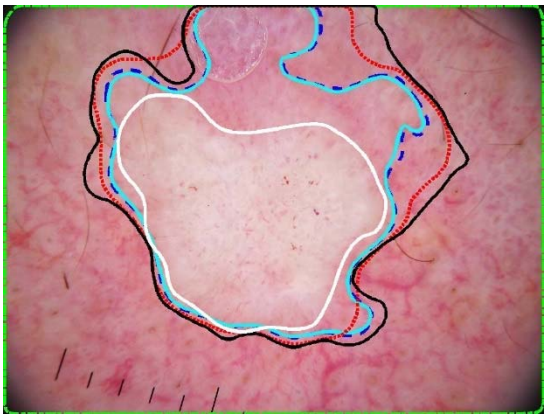

(10a)

(10b)

(10c)

Figure 10a-c: Examples for BCC lesion mask overlay for all five methods: Dashed blue – Isodata, Dashed-dotted green – Li, Solid Teal – Otsu, Dotted Red – Shanbhag-1, Solid black – Shanbhag-2, and Solid White – manual border. The borders vary widely. Note that the automatic segmentation routines often include areas outside the manual (white) border.

$$\text{Weighted XOR Error} = (1-\omega)\left(\frac{FN}{FN+TP}\right) + \omega\left(\frac{FP}{FP+TN}\right) \quad (5)$$

4 DISCUSSION

This research gives results for automatic detection of a large group of BCCs and benign lesions. Despite significant differences between the manual borders and the automatic borders, in yielding the correct diagnosis, automatically-generated lesion borders in some cases can perform slightly better than manual borders.

This study is the largest known study of automatic diagnosis performed on a set of BCCs and benign lesions. These lesions, acquired from US private practice clinics, were challenging for machine vision, as some were as small as 1mm in greatest diameter.

5 CONCLUSIONS

Sets of dermoscopy images of basal cell carcinoma can automatically be separated from images of benign lesions with moderate accuracy using the leave-one-out training and testing on 1023 lesion images and factoring in clinical data. Steps taken during this study included automatic construction of hair masks, automatic lesion segmentation, and the determination of multiple logistic regression functions: three for general dermoscopic color and structure features, two for specific basal cell carcinoma features, and one for demographic variables. Experimental results show that the automatically-determined borders perform similarly and in some cases slightly better than manually-determined borders. The hierarchical logistic regression techniques demonstrated here can perform well in separating malignant lesions from benign lesions. No single logistic regression classifier achieved the level of performance obtained when factoring together the results from the individual classifiers. This research shows that diagnostic success with machine vision does not always require accurate expert-determined borders. This research highlights the potential that the hierarchical, regression-selection process, fused with demographic data, can serve as a model for effectively diagnosing skin lesions.

ACKNOWLEDGEMENTS

This publication was made possible by Grant Number SBIR R44CA-101639-02A2 of the National Institutes of Health (NIH). The contents of this article are solely the responsibility of the authors and do not necessarily represent the official views of NIH, the sponsor.

REFERENCES

Aberg, P. et al., 2004, Skin cancer identification using multifrequency electrical impedance--a potential screening tool, *IEEE Trans Biomed Eng,* 51(12), pp.2097-2102.

Abu-Mostafa, Y.S., Magdon-Ismail, M., Lin, H.T., 2012, Learning from Data, Vol 4, AML Book, Signapore.

Ahlgrimm-Siess, V. et al., 2009, Reflectance confocal microscopy in the daily practice, *Semin Cutan Med Surg,* 28(3), pp.180-189.

Argenziano, G. et al., 1998, Epiluminescence microscopy for the diagnosis of doubtful melanocytic skin lesions: comparison of the ABCD rule of dermatoscopy and a new 7-point checklist based on pattern analysis, *Arch Dermatol*, 134(12), pp.1563-1570.

Argenziano, G. et al., 2003, Dermoscopy of pigmented skin lesions: results of a consensus meeting via the Internet, *J Amer Acad Dermatol*, 48(5), pp.679-693.

Avanaki, M.R. et al., 2013, Investigation of basal cell carcinoma using dynamic focus optical coherence tomography, *Appl Opt*, 52(10), pp.2116-2124.

Beetner, D.G. et al., 2003, Differentiation among basal cell carcinoma, benign lesions, and normal skin using electric impedance, *IEEE Trans Biomed Eng*, 50(8), pp.1020-1025.

Braun, R.P. et al., 2007, The significance of multiple blue-grey dots (granularity) for the dermoscopic diagnosis of melanoma, *Br J Dermatol*, 157(5), pp.907-913.

Castro, R.P. et al., 2015, Accuracy of in vivo confocal microscopy for diagnosis of basal cell carcinoma: a comparative study between handheld and wide-probe confocal imaging, *J Eur Acad Dermatol Venereol*, 29(6), pp.1164-1169.

Celebi, M.E., Schaefer, G., Iyatomi, H., Stoecker, W.V., 2009, Lesion Border Detection in Dermoscopy Images, *Comput Med Imaging Graph*, 33(2), pp. 148–153.

Celebi, M.E., Wen, Q., Iyatomi, H., Shimizu, K., Zhou, H., Schaefer, G., 2015, *A state-of-the-art survey on lesion border detection in dermoscopy images. Dermoscopy Image Analysis,* M. E. Celebi, T. Mendonca and J. S. Marques, Eds., Boca Raton, CRC Press, pp. 97–129.

Codella, N.C., Gutman, D., Dusza, S., Marchetti, M., Marghoob, A., Helba, B., Mishra, N., Kalloo, A., Halpern A., 2016, Skin Lesion Analysis toward Melanoma Detection, *Proceedings of the Society for Melanoma Research (SMR).*

Cheng, B. et al., 2011, Automatic detection of basal cell carcinoma using telangiectasia analysis in dermoscopy skin lesion images, *Skin Res Technol,* 17(3), pp.278-287.

Cheng, B. et al., 2012, Automatic telangiectasia analysis

in dermoscopy images using adaptive critic design, *Skin Res Technol,* 18(4), pp.389-396.

Cheng, B. et al., 2013, Automatic dirt trail analysis in dermoscopy images, *Skin Res Technol,* 19(1), pp.e20-26.

Dua, R. et al., 2004, Detection of basal cell carcinoma using electrical impedance and neural networks, IEEE *Trans Biomed Eng*, 51(1), pp.66-71.

Duan, L. et al., 2014, Automated identification of basal cell carcinoma by polarization-sensitive optical coherence tomography, *Biomed Opt Express,* 5(10), pp.3717-3729.

Eberhardt, C. et al., 2004, Early detection of skin cancer (EDISCIM) through the use of non-invasive confocal imaging, *Stud Health Technol Inform*, 103, pp.279-286.

Gambichler, T., Moussa, G., Altmeyer, P., 2008, A pilot study of fluorescence diagnosis of basal cell using a digital flash light-based imaging system, *Photo dermatol Photoimmunol Photomed*, 24(2), pp.67-71.

Gutman, D., Codella, N.C.F., Celebi, E., Helba, B., Marchetti, M., Mishra, N., Halpern, A., 2016, Skin Lesion Analysis toward Melanoma Detection: A Challenge at the International Symposium on Biomedical Imaging (ISBI) 2016, hosted by the International Skin Imaging Collaboration (ISIC), *arXiv preprint* arXiv:1605.01397.

Guvenc, P. et al., 2013, Sector expansion and elliptical modeling of blue-gray ovoids for basal cell carcinoma discrimination in dermoscopy images, *Skin Res Technol*, 19(1), pp.e532-536.

Hance, G.A., Umbaugh, S.E., Moss, R.H., Stoecker, W.V., 1996, Unsupervised color image segmentation: with application to skin tumor borders, *IEEE Eng Med Biol*, 15(1), pp. 104–111.

Heckbert, P., 1982, Color image quantization for frame buffer display, *SIGGRAPH Proceedings of the 9th annual conference on Computer Graphics and Interactive Techniques*, 82, pp.297-307.

Huang, L.K., Huang, M.J., 1995, Image thresholding by minimizing the measures of fuzziness, *Pattern Recognition*, 28(1), pp.41-51.

Jella, P., 2004, Pigment network extraction and salient point analysis. M.S. Thesis in Electrical Engineering, University of Missouri, Rolla, MO, USA.

Kasmi, R., 2016, Biologically inspired Skin lesion segmentation process, Ph.D. Dept. Elect. Eng., Univ. Bejaia, Bejaia, Algeria.

Kaur, R., LeAnder, R., Mishra, N.K., Hagerty, J.R., Kasmi, R., Stanley, R.J., Celebi, M.E., Stoecker, W.V., 2016, Thresholding methods for lesion segmentation of basal cell carcinoma in dermoscopy images, *Skin Research and Technology*, 2016, doi: 10.1111/srt.12352 (in press).

Kaushik, V.S.N. et al., 2013, The Median Split Algorithm for Detection of Critical Melanoma Color Features, *VISAPP,* 1, pp.492-495.

Kefel, S. et al., 2012, Discrimination of basal cell carcinoma from benign lesions based on extraction of ulcer features in polarized-light dermoscopy images, *Skin Res Technol,* 18(4), pp.471-475.

Kefel, S., Kefel, S.P., LeAnder, R.W., Kaur, R., Kasmi, R., Mishra, N.K., Rader, R.K., Cole, J.G., Woolsey, Z.T., Stoecker, W.V., 2016, Adaptable texture-based segmentation by variance and intensity for automatic detection of semitranslucent and pink blush areas in basal cell carcinoma, *Skin Research and Technology*, 22(4), pp. 412-422.

Kopriva, I. et al., 2007, Visualization of basal cell carcinoma by fluorescence diagnosis and independent component analysis, *Photodiagnosis Photodyn Ther*, 4(3), pp.190-196.

Landini, G., 2013, http://fiji.sc/Auto_Threshold#Li v1.15.

Larraona-Puy, M. et al., 2009, Development of Raman microspectroscopy for automated detection and imaging of basal cell carcinoma, *J Biomed Opt*, 14(5), 054031.

Li, C.H., Tam, P.K., 1998, An iterative algorithm for minimum cross entropy thresholding, *Pattern Recog Lett,* 19(8), pp.771-776.

Ly, E. et al., 2009, Differential diagnosis of cutaneous carcinomas by infrared spectral micro-imaging combined with pattern recognition, *Analyst,* 134(6), pp.1208-1214.

Marghoob, A.A., Malvehy, J., Braun, F.P., 2012, An Atlas of Dermoscopy, *2nd Edition, Boca Raton FL*:CRC Press.

Mishra, N., 2014, Automated classification of malignant melanoma based on detection of atypical pigment network in dermoscopy images of skin lesions. Ph.D. Thesis, Department of Electrical and Computer Engineering, Missouri University of Science and Technology, Rolla, MO.

Mishra, N.K., Celebi, M.E., 2016, An overview of melanoma detection in dermoscopy images using image processing and machine learning, *arXiv preprint* arXiv:1601.07843.

Moss, R.H. et al., 1989, Skin cancer recognition by computer vision, *Comput Med Imaging Graph*, 13(1), pp.31-36.

Nijssen, A. et al., 2002, Discriminating basal cell carcinoma from its surrounding tissue by Raman spectroscopy, *J Invest Dermatol,* 119(1), pp.64-69.

Otsu, N., 1979, A threshold selection method from grey level histograms, *IEEE Trans Systems, Man, Cybern*, 9(1), pp.62-66.

Riddler, T.W., Calvard, S., 1978, Picture thresholding using an iterative selection method, *IEEE Trans Systems, Man, Cybern*, 8, pp. 630-632.

Rogers, H.W. et al., 2010, Incidence estimate of nonmelanoma skin cancer in the United States, 2006. *Arch Dermatol,* 146(3), pp.283–287.

Rogers, H.W., Coldiron, B.M., 2013, Analysis of skin cancer treatment and costs in the United States Medicare population, 1996-2008, *Dermatol Surg*, 39(1 Pt 1), pp.35-42.

Sforza, G., Castellano, G., Arika, S.K., Leander, R.W., Stanley, R.J., Stoecker, W.V., Hagerty, J.R., 2012, Using adaptive thresholding and skewness correction to detect gray areas in melanoma in situ images, *IEEE*

Trans Instrum Meas, 61(7), pp. 1839–1847.

Shanbhag, A.G., 1994, Utilization of information measure as a means of image thresholding, *CVGIP: Graph Models Image Proc*, 56(5), pp.414-419.

Soyer, H.P., Argenziano, G., Hofmann-Wellenhof, R., Johr, R. (eds), 2007, *Color Atlas of Melanocytic Lesions of the Skin*, Berlin, Germany: Springer Berlin Heidelberg.

Steger, C., 1996, Extracting lines using differential geometry and Gaussian smoothing, *Int Arch Photogrammetry Remote Sensing,* 31, pp.821-826.

Stoecker, W.V., et al., 2009, Semitranslucency in dermoscopic images of basal cell carcinoma, *Arch Dermatol,* 145(2), pp.224.

Stoecker, W.V., Mishra, N., LeAnder, R., Rader, R., Stanley, R., 2013, Automatic Detection of Skin Cancer – Current Status, Path for the Future, *In: Proceedings of the International Conference on Computer Vision Theory and Applications*, pp. 504-508. Available: https://goo.gl/7o5JfY.

Stoecker, W.V., Mishra, N.K., Kaur, R., Kasmi, R., Cole, J.G., Safron, A., Moss, R.H., Leander, B., Stanley, R.J., Rabinovitz, H., Oliviero M., 2015, Automatic Diagnosis of Basal Cell Carcinoma: Fusion of Dermoscopic and Clinical Features, *American Academy of Dermatology Symposium*, At Nob Hill ABC, Marriott Marquis San Francisco San Francisco, CA, USA.

Stolz, W. et al., 2002, *Color Atlas of Dermatoscopy*, 2nd Edition, Berlin: Blackwell Science.

Tehrani, H. et al., 2007, Spectrophotometric intracutaneous analysis in the diagnosis of basal cell carcinoma: a pilot study, *Int J Dermatol*, 46(4), pp.371-375.

Umbaugh, S.E., Moss, R.H., Stoecker, W.V., 1989, Automatic color segmentation of images with application to detection of variegated coloring in skin tumors, *Eng Med Biology Magazine IEEE*, 8(4), pp.43-50.

Umbaugh, S.E., 2010, *Digital Image Processing and Analysis: Human and Computer Vision Applications with CVIPtools,* Boca Raton FL, CRC press.

Won, Y. et al., 2007, Photodetection of basal cell carcinoma using methyl 5-aminolaevulinate-induced protoporphyrin IX based on fluorescence image analysis, *Clin Exp Dermatol,* 32(4), pp.423-429.

Zeichner, J.A., Patel, R.V., Birge, M.B., 2011, Treatment of Basal cell carcinoma with curettage followed by imiquimod 3.75% cream, *J Clin Aesthet Dermatol*, 4(5), pp.39-43.

Zhang, J. et al., 2000, A feasibility study of multispectral image analysis of skin tumors, *Biomed Instrum Technol,* 34(4), pp.275-282.